# FINAL REPORT

**NETWORK-H2**
**CALL 2 - OPEN**

## PROJECT DETAILS

**Grant number**

| |
|---|
| NH2-006 |

**Award holding organisation**

| | |
|---|---|
| Organisation | Edinburgh Napier University |

**Title of research project**

| |
|---|
| Computational analysis of a zero-carbon hydrogen fuelled thermal engine for heavy duty transport applications |

**Investigators**

| Role | Name | Organisation |
|---|---|---|
| Principal investigator | Dr Efstathios-Al. Tingas | Edinburgh Napier University |
| Co-investigator | Professor Manosh Paul | University of Glasgow |

**Grant number**

NH2-006

**Final Project Report (up to 10 A4 pages)**

Task 1.1 from WP1 was already presented in the interim report. The results were published in Int. J. Hydrog. Energy 47:17 (2022) 10083-1009, doi: 10.1016/j.ijhydene.2022.01.093
In the current report, we summarise the findings from Task 1.2 (led by the PI, ENU) as well as WP2 (led by the co-PI, UoG).

WP1: HCCI Engine Simulations – Task 1.2 (led by the PI, ENU)
The results from this analysis were recently published in Fuel 326 (2022) 125100 (10.1016/j.fuel.2022.125100), hence here only a brief description will be provided.
The addition of hydrogen peroxide and steam to a hydrogen-fuelled HCCI engine was investigated at various fuel lean conditions (φ= 0.2–0.6) and compression ratios (15–20) using a 0-dimensional numerical model. The use of hydrogen peroxide as an ignition promoter demonstrated increased IMEP (16%–39%), thermal efficiency (up to 2%), and reduced NOx (50%–76%) when compared to the conventional method of intake charge heating. When hydrogen peroxide was used as an ignition promoter, a 15% addition of steam was sufficient to reduce NOx by 93%–97%, though this reduced IMEP and thermal efficiency slightly. When heat transfer was considered and steam addition was increased from 0%–10%, no increase in intake air heating was able to match the IMEP of 5% hydrogen peroxide addition without an increase in the equivalence ratio (up to 40%). The parametric space of hydrogen peroxide (0%–25%) and steam (0%–40%) addition was explored in view of engine performance metrics, showing the complete range of conditions possible through control of both inputs. A three-order reduction in NOx was possible through steam addition. An optimal balance of performance and emissions occurred at 5%–10% hydrogen peroxide and 10%–15% steam addition. In a study of compression ratio, very little hydrogen peroxide addition (5%) was required to achieve 98% of the maximum efficiency at higher compression ratios (19–20), though at lower compression ratios (17) impractical quantities of hydrogen peroxide were required. The 10% steam addition present at these conditions led to extremely low NOx levels for of 0.3 and 0.4, though at of 0.5 NOx levels would require some after-treatment. Maintaining constant a high or low load across steam additions was possible through reasonable adjustment of hydrogen peroxide addition.

WP2: Dual fuel CI engine simulations (led by the co-PI, UoG)

**Engine Model**
Simulation of the engine is achieved using a zero-dimensional, time dependant model of a piston-cylinder system. For convenience, model calculations are completed in the crank angle domain, θ, which correlates to the time domain through the engine's angular velocity, ω.
The principal parameters governing this model are the differential equations of the system pressure and the system volume. A first-law analysis of the ideal gas piston-cylinder system is the basis for the derived expression of pressure with respect to crank angle shown in equation (1). This approach considers heat generated from combustion, Qc, heat lost to the cylinder wall, QL, and latent heat of the vaporising injection mixture, hi (Heywood, 1988; Ferguson & Kirkpatrick, 2016).

$$\frac{dP}{d\theta} = \frac{\gamma - 1}{V} \cdot \left(\frac{dQ_c}{d\theta} - \frac{dQ_L}{d\theta}\right) + \frac{\gamma - 1}{V}(\Delta h_i) \cdot \frac{dm_i}{d\theta} - \frac{\gamma \cdot P}{V} \cdot \frac{dV}{d\theta} \quad (1)$$

An expression for the system's volume is derived from the specified geometry of the engine's cylinder, crankshaft, and connecting rod.

$$V(\theta) = V_c + \frac{V_c}{2}(r_c - 1) \cdot \left(1 - \cos(\theta) + \frac{\epsilon}{2}\sin^2(\theta)\right) \quad (2)$$

$$\therefore \frac{dV}{d\theta} = \frac{V_c \cdot (r_c - 1)}{2}\sin(\theta) \cdot (1 + \epsilon\cos(\theta))$$

The simulation is run over the range of crank angles from -180 CAD to 180 CAD, covering the compression and power strokes of the engine cycle. A fourth order Runge-Kutta method is used to

determine the cylinder pressure while other system properties are calculated explicitly. Indicated cycle work is calculated using the pressure and volume data as $W = \int_{\theta} P\, dV$.

**Hydrogen Peroxide Injection**

For each model case, the concentration of the aqueous H2O2 solution and the H2O2/fuel injection ratio are set a priori along with the specified injection timings for injection start and injection duration, θi and Δθ. Injection of the peroxide solution happens at a constant mass flow rate over the prescribed cycle interval, Δθ. The cylinder gas mixture is always assumed to remain homogenous, and the injected solution is therefore assumed to instantly vaporise upon induction into the cylinder. Thermodynamics of this phase change are accounted for via the vaporisation enthalpy change term in the pressure differential equation.

## Combustion Model

**Weibe function**

Progress of the combustion reaction is approximated using a Weibe function to determine the fraction of cylinder charge that has burned. The form of the Weibe function is given in equation (4).

$$X_b = \frac{m_b}{m_t} = \frac{\text{burned mass}}{\text{total charge mass}} = \frac{Q_c}{\Delta H_c} \tag{3}$$

$$X_b(\theta) = 1 - \exp^{-c_1\left(\frac{\theta-\theta_i}{\Delta\theta}\right)^{c_2}} \tag{4}$$

$$\frac{dX_b}{d\theta} = \left(\exp^{-c_1\left(\frac{\theta-\theta_s}{\theta_d}\right)^{c_2}}\right)\cdot\frac{(c_1\cdot c_2)}{\Delta\theta}\cdot\left(\frac{\theta-\theta_i}{\Delta\theta}\right)^{c_2-1} = (1-X_b)\cdot\frac{c_1\cdot c_2}{\Delta\theta}\cdot\left(\frac{\theta-\theta_i}{\Delta\theta}\right)^{c_2-1} \tag{5}$$

$$\frac{dQ_c}{d\theta} = \Delta H_c\cdot\frac{dX_b}{d\theta} = \Delta H_c\cdot(1-X_b)\cdot\frac{c_1\cdot c_2}{\Delta\theta}\cdot\left(\frac{\theta-\theta_s}{\Delta\theta}\right)^{c_2-1} \tag{6}$$

For traditionally fuelled engines, values for constants $c_1$ and $c_2$ are taken as 5 and 3, respectively. Hydrogen fuelled engines have different combustion properties and thus would require different Weibe parameters to approximate the process. In the present work, a preliminary evaluation of the combustion characteristics of differing gas mixtures is used to determine representative Weibe parameters to approximate their combustion in an engine.

**Kinetic combustion data**

A series of Chemkin simulations generated combustion data for hydrogen/hydrogen peroxide solution mixtures under a HCCI regime. This method of simulation tracks the progress of chemical reactions based on a set of kinetic mechanisms to determine combustion properties over the compression and expansion strokes of a compression-ignition engine cycle. The fundamental mechanisms used in these models are consistent with previous studies on the performance of hydrogen/hydrogen peroxide blends in HCCI combustion regimes (Dimitrova, Megaritis, Ganippa, & Tingas, 2022). Outputs of these simulations include pressure and temperature profiles and the calculated heat release rate (HRR) due to the combustion reactions.

Integrating the generated HRR curve and normalising the result by the total combustion heat released yields the mass burn fraction (MFB). This is the parameter that is approximated by the Weibe function, thus numerical simulation of the in-cylinder combustion reaction can yield data that allows for fitting a representative Weibe function to model the process.

**Weibe parameter fitting**

The first parameters derived from the generated combustion profiles are the start of combustion, $\theta_i$, and the combustion duration, Δθ. The combustion process was assumed to take place between MFBs of 1% and 98% thus $\theta_i$ is the CAD read from the MFB curve and Δθ is determined from the difference between the CAD at combustion start and combustion end on the same curve. Furthermore, the ignition temperature corresponds to the generated temperature data at the $\theta_i$ CAD.

Remaining Weibe parameters are determined using the methods of Yeliana et al. (2011) by first substituting an intermediate parameter, α, into the Weibe function and linearising the equation.

$$\alpha = \Delta\theta \cdot c_1^{-1/c_2} \quad \therefore X_b = 1 - \exp\left(-\left(\frac{\theta - \theta_i}{\alpha}\right)^{c_2}\right) \tag{7}$$

$$\ln(-\ln(1 - X_b)) = c_2 \cdot [\ln(\theta - \theta_i) - \ln(\alpha)] \tag{8}$$

Equation (8) represents the linearised MFB function where the parameter c2 is the slope and the intercept is ln(α)/c2. These parameters are then estimated by performing a linear regression on data points taken from the MFB generated from the kinetic simulation.
An example comparing the MFB derived from a kinetic simulation with its representative Weibe function is presented in Figure 1. This case used 12.02%v H2, 1.14%v H2O2, 18.00%v H2O, 54.38%v N2, and 14.46%v O2 as the intake fuel/air mixture corresponding to a 9.5% H2O2/H2 ratio using a 6% H2O2(aq) solution at an effective equivalence ratio (Dimitrova, Megaritis, Ganippa, & Tingas, 2022) of 0.4. In general, the derived Weibe function demonstrates good alignment with the numerically derived MFB curve, particularly during the region of rapid combustion ~2.0-3.6 CAD, corresponding to the final 90% of the combustion process.

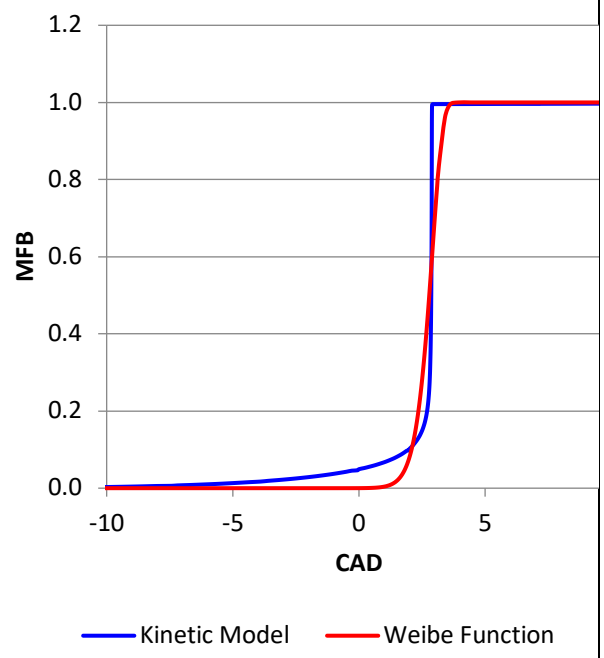


Figure 1: Comparison of combustion profiles calculated from a kinetic combustion model and the derived Weibe function (9.5%mol. $H_2O_2/H_2$; 6%mol. $H_2O_{2(aq)}$; 0.4 equivalence ratio)

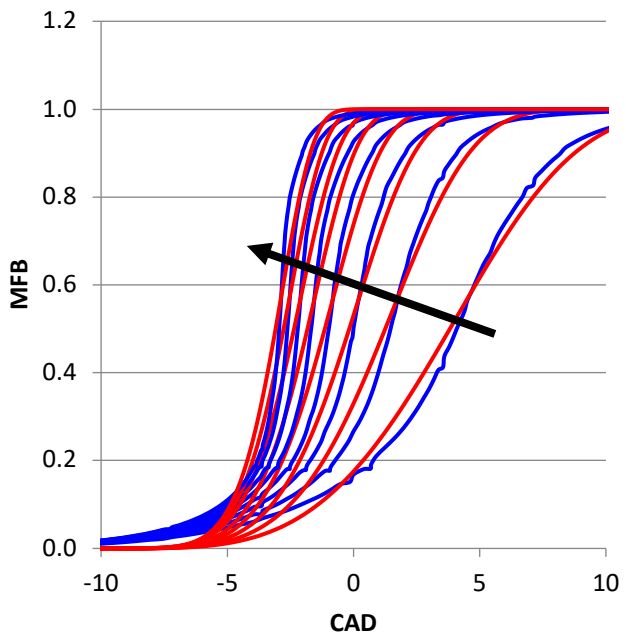


Figure 2: Variation in kinetic MFB profiles (blue) and derived Weibe functions (red). Arrow shows trend of increasing $H_2O_2$ injection ratio. (equivalence ratio 0.2)

**Parameter Variation**

Data from the kinetic simulations also illustrate some variation in combustion profiles depending on the gas mixtures analysed (Figure 2). To account for this behaviour, a strategy of using adaptive Weibe function parameters is implemented (Alam & Depcik, 2019). Correlations for each parameter were established as the peroxide solution injection ratio increased at given concentrations and equivalence ratios. These correlations were ultimately calculated in terms of the hydrogen peroxide molar fraction in the reacting mixture.
Figure 3 illustrates the observed trends in Weibe parameters for two different concentrations of H2O2(aq) solution at an equivalence ratio of 0.4. Considering the modelled system is a compression-ignition whereby heat to initiate the combustion reaction comes from the temperature rise associated with gas compression, the mixture temperature at ignition is tracked rather than the respective $\theta_i$. For both peroxide concentrations, the ignition temperature decreased as more H2O2(aq) was added to the system, highlighting the combustion promoting properties of this compound.

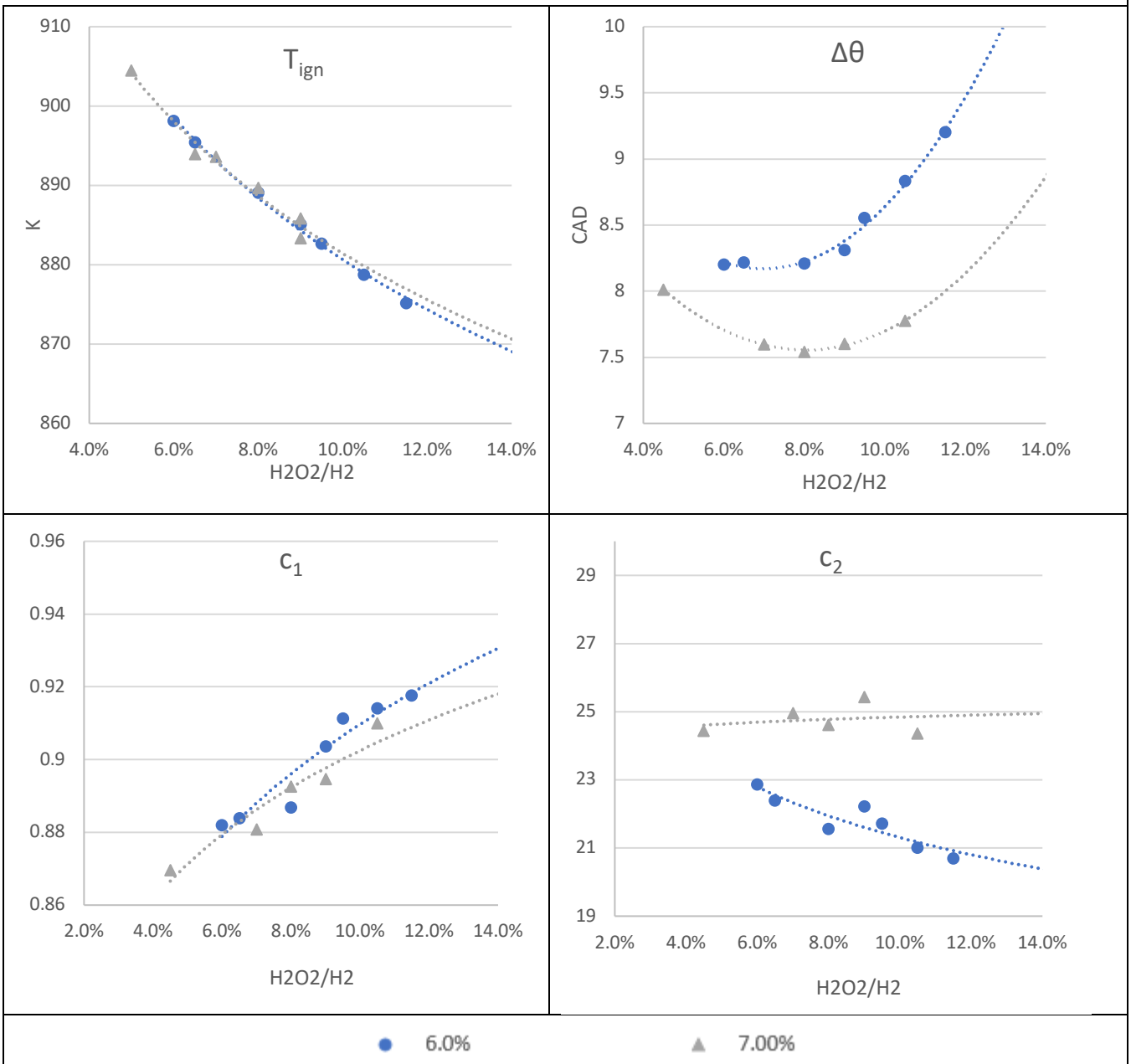


Figure 3: Variations of Weibe parameters for ignition temperature, combustion duration, and correlation constants with $H_2O_{2(aq)}$ injection for 6% and 7% solution concentrations

**Simulation Details**

Fortran subroutines are used to run the simulation program, a summary of which follows. Figure 4 illustrates a simplified flowchart of the process. The initial fuel/air mixture composition, intake temperature and pressure, initial volume, thermophysical properties, MFB, CAD, and residual exhaust fraction ($x_r$) are initialised. A do loop uses a fourth order Runge-Kutta method to solve the pressure differential equation and advance to the next CAD step and the cylinder temperature is calculated using the equation of state. If the current CAD is within the range specified for H2O2(aq) injection, the mass flow of solution and heat of vaporisation are calculated and stored to memory.

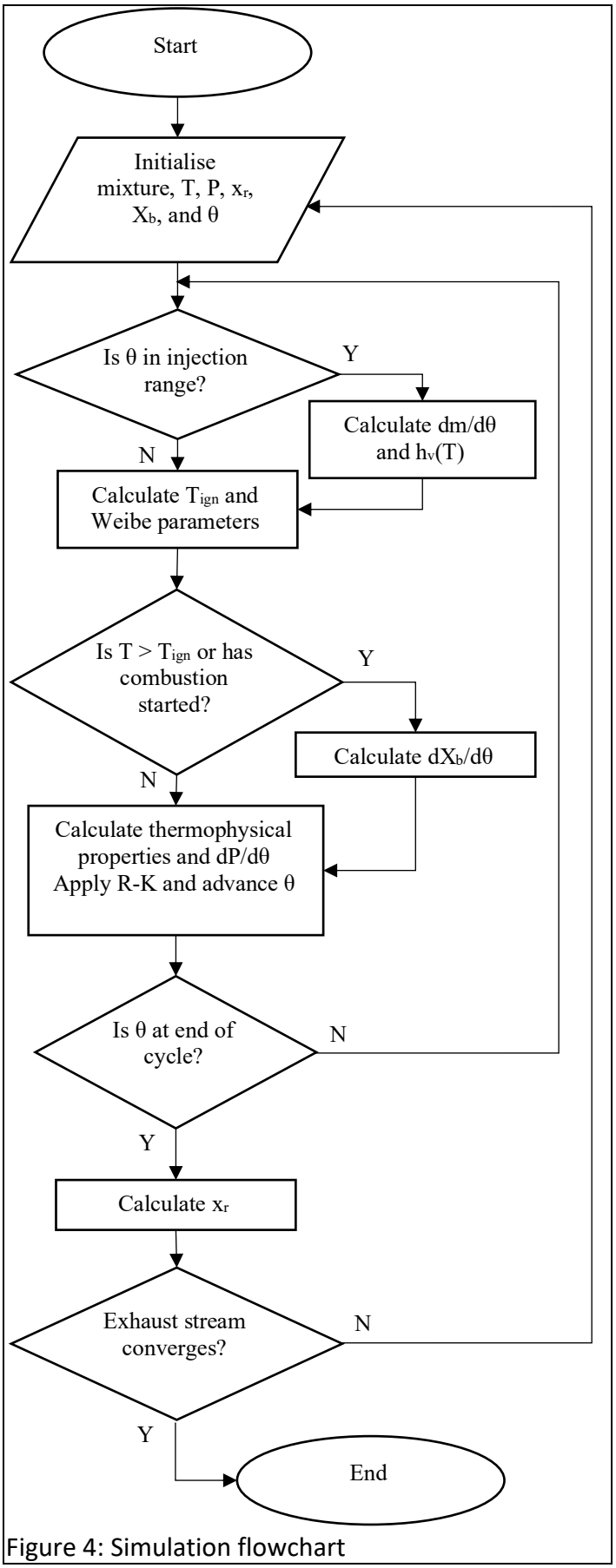

Figure 4: Simulation flowchart

The gas mixture is updated to include the newly injected species. Using the derived Weibe parameter correlations and the latest hydrogen peroxide fractions, values for $\Delta\theta$, $c_1$, $c_2$, and the ignition temperature are calculated and stored to memory.

Next, the model determines whether the mixture is in the combustion regime. This condition is triggered if the current temperature exceeds the calculated ignition temperature of if the combustion process has previously been initiated. When the combustion criterion is first met, the current CAD step is saved to memory as the ignition angle, $\theta_i$, in the Weibe function. If the current step is further advanced than $\theta_i$ then the Weibe function calculates $X_b$ and $dX_b/d\theta$.

Using the combustion data, the gas mixture is updated to account for fuel and oxygen consumed and then the thermophysical properties are recalculated. If the current CAD step has not reached the end of the simulated cycle the do-loop repeats, advancing to the CAD step, recalculating and solving the pressure equation and equation of state.

If the do-loop has reached the end of the cycle, cylinder blow down is calculated to determine the exhaust temperature and pressure. The residual exhaust fraction is then calculated. A final convergence test compares the exhaust temperature, pressure, and species to the results of the preceding simulation cycle. If the simulation is unconverged, the cycle is reinitialised using the latest residual mass fraction to augment the new intake mixture. Once the cycle converges, the program integrates the pressure and volume arrays and outputs the indicated cycle work.

**Method validation**

To assess the ability of the derived model to represent a realistic hydrogen combustion scenario, a validation case was established based on experimental data (Sathishkumar & Ibrahim, 2021). There are currently no experimental studies on $H_2/H_2O_2$ combustion in an internal combustion engine therefore the reference study on $H_2$/diesel HCCI is taken as a representative case. To make the most effective comparison to our $H_2$ combustion model, the highest hydrogen energy share (HES) case of 27% was selected from the reference work.

The engine used in the experiment has dimensions reported in Table 1. The fuel mixture was a combination of $H_2$ and diesel such that 27% of the supplied energy came from $H_2$ combustion, on a LHV basis. Engine intake conditions were 2 bar and 400 K. Following the described method, a Chemkin simulation using the same parameters was used to determine the combustion characteristics and Weibe parameters based on the experimental set up. This simulation assumed *n*-heptane was an acceptable surrogate for diesel fuel for the purposes of the chemical kinetic calculations.

Table 1: Validation engine parameters

| | |
|---|---|
| Compression ratio: | 18.5:1 |
| Displacement volume: | 909 $cm^3$ |
| Bore: | 83 mm |
| Stroke: | 84 mm |
| No. of cylinders: | 2 |
| Connecting rod: | 140.5 mm |
| Speed: | 1800 RPM |

Figure 5 compares the model simulation outputs to the data from the experimental case. In general, there are important similarities in these data that support the validity of the numerical methods used. The average rate of pressure rise of 4.35 bar/CAD calculated by our model is moderately higher than the 3.18 bar/CAD reported in the study, however it is within the range of some experimental cases using a higher proportion of diesel fuel. While these discrepancies in scale can be noted, consideration of the nature of the experimental data would lead one to expect such differences between the figures. In the first place, the experimental data was collected from the observed cylinder pressures and brake power output from the test engine and then details of the HRR were calculated. In this way, the absolute magnitude of the experimental HRR is affected by heat losses and friction losses which could cause losses on the order of 40-50% of the input energy. On the other hand, the HRR in the numerical model is calculated directly based on the thermodynamics and kinetic progress of the combustion reaction. Furthermore, the kinetic model was calculated using an adiabatic assumption meaning more heat remains within the reacting system. As a final note, the authors also indicated there was evidence of incomplete diesel vaporisation during these experiments, meaning less chemical energy was actually delivered to the cylinder charge than was input with the fuel. This difference between the indicated parameters calculated from the numerical simulation and the brake values measured along with the disparity between the adiabatic and heat loss scenarios combine to make the experimental data for HRR and cylinder pressure lower than for the idealised scenario analysed in the numerical model.

Therefore, despite the apparent discrepancies in absolute scale between the numerical and experimental cases, we examine instead the timings and relative progress of the combustion reactions. Given the focus of the present study is a comparison of $H_2O_{2(aq)}$ injection schemes rather than an absolute performance assessment of such an engine. This relative comparison is more clearly highlighted by examining the normalised data for pressure and HRR.

In terms of combustion phasing, there is good agreement for the start of combustion (~-5CAD BTDC), the peak HRR (~4CAD ATDC), and the overall combustion duration (~20CAD). This trend is also evident in the agreement in MFB and normalised pressure, particularly during the beginning of combustion. There is a small but noticeable trend that the experimental MFB, and consequently the pressure trace, begin to lead the numerically derived combustion progress. Even this region of faster fuel burn can be qualitatively explained by the documented issue of incomplete diesel vaporisation in the experiment (Sathishkumar & Ibrahim, 2021), meaning the actual $H_2$ fraction in the combustible gas mixture was higher than reported based on the reported fuel inputs. Since the laminar flame speed of $H_2$ is faster than that of diesel by roughly a factor of 10, we would expect the relatively $H_2$-enriched experimental mixture to burn slightly quicker than the numerical fuel mixture calculated based on the measured fuel inputs. Thus the sharper HRR profile, the faster MFB progress, and the leading pressure peak in the experimental data can be partially justified considering this known difference.

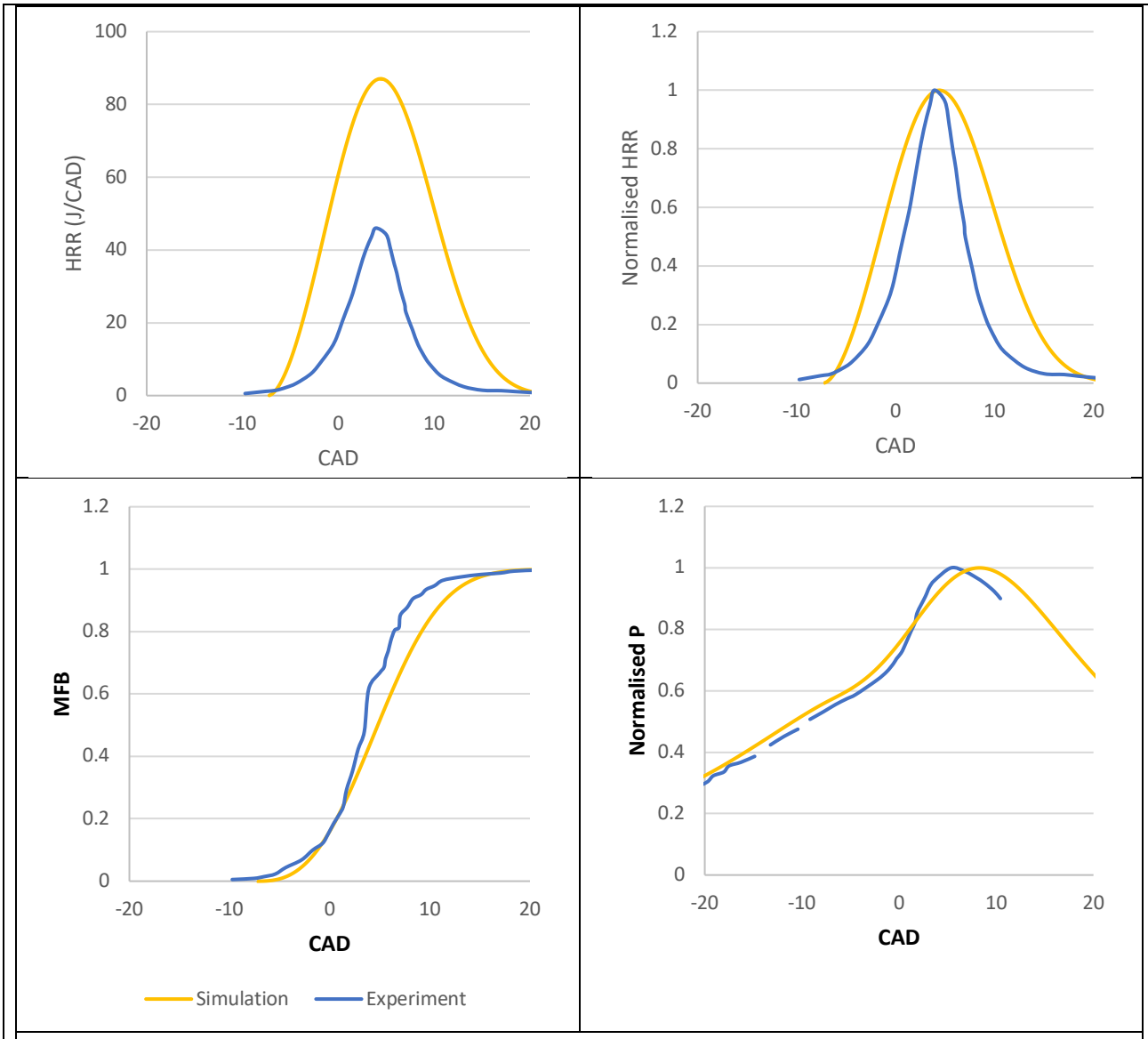


Figure 5: Comparison of model and experimental (Sathishkumar & Ibrahim, 2021) heat release rate, normalised heat release rate, mass fraction burned, and normalised cylinder pressure.

**Study of $H_2O_2$ Injection Timings**

A preliminary case is set up to provide a baseline of comparison for engine performance. Using the geometry of a typical compression-ignition cylinder as shown in Table 2 (Dimitrova, Megaritis, Ganippa, & Tingas, 2022) and initialising the cylinder with $H_2$/air to give an effective equivalence ratio of 0.4. Injection parameters were set for an early injection at -50CAD BTDC over a 5CAD injection interval to provide an early combustion scenario similar to an HCCI case. Peroxide solution concentration is set as 6% by volume and the total injection is set to give a $H_2O_2/H_2$ ratio of 6.5%molar.

Table 2: Simulated engine parameters

| | |
|---|---|
| Compression ratio: | 18:1 |
| Bore: | 100 mm |
| Stroke: | 105 mm |
| Rod/Crank: | 3.714286 |
| Speed: | 1500 RPM |
| Intake Pressure: | 1 bar |
| Intake Temperature: | 320 K |

From the data presented in Figure 6, the mixture is compressed to ignition temperature between -20~-15CAD BTDC. Combustion of the mixture completed around -10CAD BTDC with peak cylinder pressure occurring near TDC. Indicated power calculated from this cylinder cycle was 6.78 kW, thus creating an IMEP of 659 kPa.

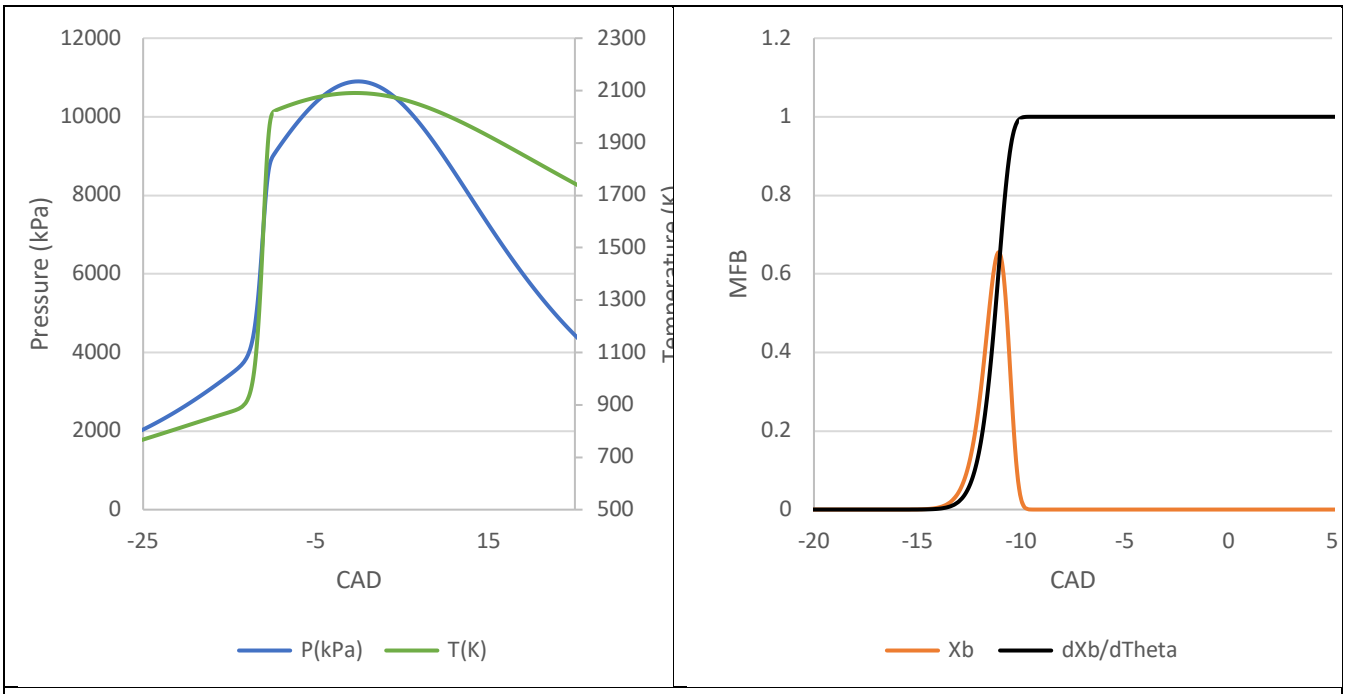


Figure 6: Pressure and temperature traces (left) and HRR and MFB (right) for baseline simulation (6.5% $H_2O_2/H_2$; 6.0%vol. $H_2O_{2(aq)}$)

A further range of simulations were executed to determine the effect of injection timing on the IMEP generated in the cylinder system. Equivalence ratio, H2O2/H2 ratio, H2O2(aq) concentration, and engine speed were all maintained constant while the injection start ranged from -20CAD≤ $\theta_i$≤10CAD and the injection interval ranged from 1CAD≤ $\Delta\theta$≤25. For comparison purposes, the calculated IMEP was normalised with reference to the preliminary HCCI IMEP. Results of this investigation are presented in Figure 7.

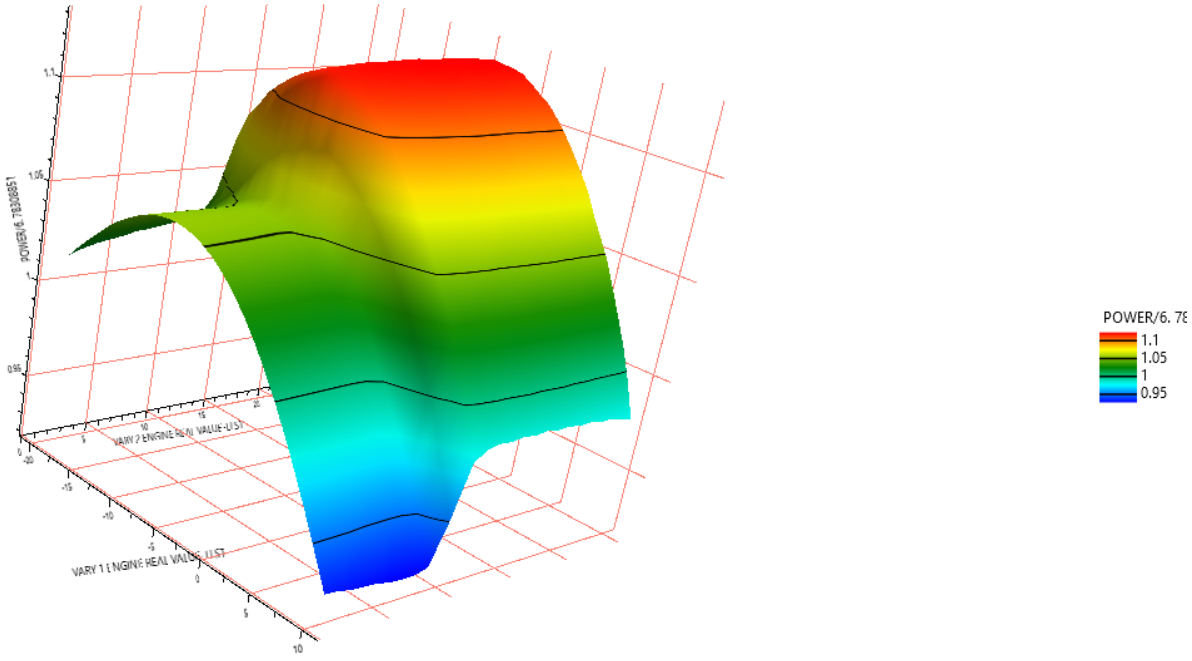


Figure 7: Variation in relative cylinder IMEP due to $H_2O_2$ injection timing and duration.

These findings indicate in the first place that the combustion performance of the $H_2$ fuelled cylinder can be influenced by the controlled injection of hydrogen peroxide during the end of the compression stroke. In general, peroxide injections from -20CAD up to 3CAD ATDC generated higher IMEPs than

the reference model case. Some injection timings as late as 8CAD ATDC could perform on par with the reference case provided a sufficiently long injection duration. Furthermore, an optimum injection timing appears to be between -8 and -9CAD BTDC.
Additionally, there appears to be a benefit to extending the injection duration beyond 10CAD. A significant jump in IMEP appears for all injection timings as the injection duration extends past the 10CAD threshold, however this effect appears to have diminishing returns. For example, the -8CAD injection time progresses from a 5.9% IMEP improvement for a 9 CAD injection interval to an 11.6% IMEP improvement for an 11 CAD injection interval. The best IMEP performance of a 12.3% increase occurs for an injection interval of 19CAD, however all intervals over 13CAD led to IMEP improvements of at least 12% for the -8CAD injection timing.
Combustion initiated by the -8CAD timing provides the ideal pressure profile for maximising the cycle work during the expansion stroke, and thus improving IMEP. Figure 8 shows this effect since the rapid period of pressure rise is just after the piston TDC, peaking at 1.8CAD ATDC in this case and ensuring the maximum cylinder pressure during the expansion stroke. In contrast, the 0CAD injection pressure profile develops well after TDC, losing out on ~10CAD of net piston work at the start of the expansion stroke. Finally, the -15CAD injection timing, like the baseline HCCI case, creates a pressure profile where combustion happens before piston TDC. This ultimately means the piston will expend extra work pushing against the high-pressure charge during the end of the compression stroke. Here, the -15, -8, and 0 CAD injection timings ultimately led to normalised IMEPS of 1.106, 1.121, and 1.054 respectively.

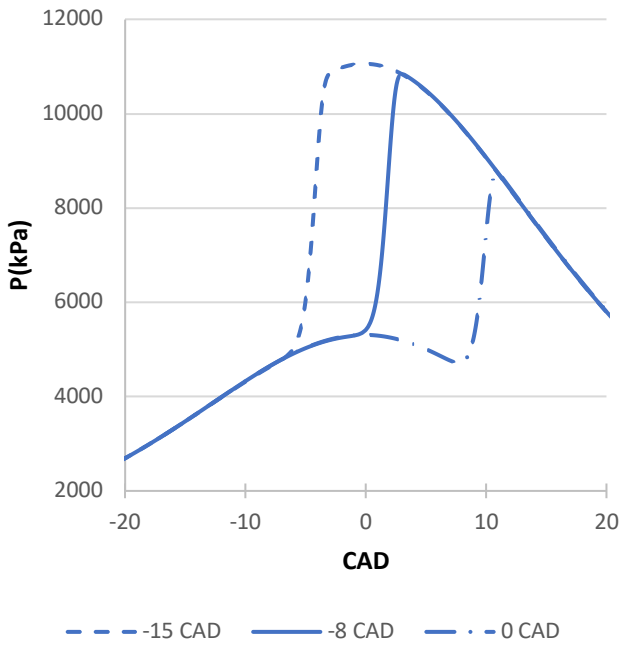


Figure 8: In-cylinder pressure profiles for three different injection schedules. All injection durations are 15CAD.

Additional insight into this process is garnered by examining the effect of injection duration. As shown in Figure 9 for the -8CAD injection timing, the HRR profile for the longer injection durations tend to skew to the left, meaning the combustion heat in these cases is released earlier and faster than in the shorter duration. Such combustion behaviour will ensure higher pressures at the start of the expansion stroke and help to increase the work developed during the piston's down stroke in this case. This result is a cause of the combustion property correlations established previously and shown in Figure 3. For the 6% $H_2O_{2(aq)}$ solution, the combustion duration and $c_2$ parameters tend to increase as more solution is included in the combustion mixture, making for a slower combustion reaction. Longer injection periods in these cases mean that the peroxide content of the mixture remains relatively low during the initial combustion phase, in contrast to the short injection intervals which will have a significant amount of peroxide present from the start of combustion. Therefore, there appears to be a balance where sufficient peroxide is injected to lower the ignition temperature while maintaining a combustion profile capable of maximising the IMEP.
Furthermore, the short injection periods require higher mass flow rates into the cylinder system. This

has the effect of both elevating the cooling effect of vaporisation and increasing the thermal mass of the system, both effects that further slow the pressure rise. All-in-all, the trends discussed here resulted in relative IMEPs of 1.053, 1.084, 1.121, and 1.122 for the 5 CAD, 10 CAD, 15 CAD, and 20 CAD injection intervals, respectively. This type of behaviour is perhaps due to the dilute peroxide solution used in this study. Figure 3 shows a stronger, 7% $H_2O_{2(aq)}$ solution has different combustion properties and even stronger concentration would likely have different properties again.

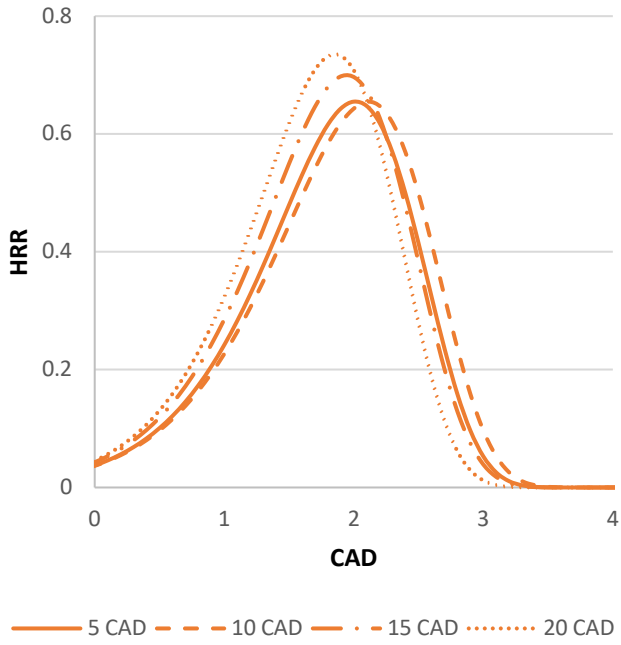


Figure 9: Combustion HRR profiles for different injection durations for injection timing of -8 CAD.

## Conclusions

- Use of kinetic models to derive correlations for combustion parameters appears to be a suitable method to model a hydrogen fuelled, hydrogen peroxide injected, compression ignition engine.
- Hydrogen peroxide injection may be an effective method to control the combustion of a $H_2$ fuelled compression ignition engine. This is limited to injection within -20 to 20 CAD for the current study. Earlier injections will result in an HCCI mode of combustion with later injections will not have sufficient cylinder temperature to initiate combustion.
- Control of combustion timing can enhance the engine cycle IMEP. In the current study, cycle IMEP could increase by 12.3% over the uncontrolled HCCI case by injecting hydrogen peroxide starting at -8 CAD BTDC over an interval of at least 15 CAD.

## References

Alam, S. S., & Depcik, C. (2019). ADAPTIVE WIEBE FUNCTION PARAMETERS FOR A PORT-FUEL INJECTED HYDROGEN-FUELED ENGINE. *Proceedings of the ASME 2019 International Mechanical Engineering Congress and Exposition.* Salt Lake City: ASME.

Dimitrova, I., Megaritis, T., Ganippa, L. C., & Tingas, E. (2022). Computational analysis of an HCCI engine fuelled with hydrogen/hydrogen peroxide blends. *International Journal of Hydrogen Energy, 47*, 10083-10096. doi:10.1016/j.ijhydene.2022.01.093

Ferguson, C. R., & Kirkpatrick, A. T. (2016). *Internal Combustion Engines Applied Thermosciences* (3rd ed.). Chichester: John Wiley & Sons.

Heywood, J. B. (1988). *Internal Combustion Engine Fundamentals.* New York: McGraw-Hill.

Sathishkumar, S., & Ibrahim, M. (2021). Comparison of the hydrogen powered homogeneous charge compression ignition mode with multiple injection schedules and the dual fuel mode using a twin-cylinder engine. *International Journal of Hydrogen Energy, 46*, 1315-1329. doi:10.1016/j.ijhydene.2020.10.032

Yeliana, Cooney, C., Worm, J., Michalek, D., & Naber, J. (2011). Estimation of double-Wiebe function parameters using least square method for burn durations of ethanol-gasoline blends in spark ignition engine over variable compression ratios and EGR levels. *Applied Thermal Engineering, 31*, 2213-2220. doi:10.1016/j.applthermaleng.2011.01.040

| | |
|---|---|
| $T$ | Temperature (K) |
| $R$ | Gas constant (kJ/mol-K) |
| $C_p$ | Heat capacity (kJ/mol-K) |
| $r_c$ | Compression ratio (-) |
| $m$ | Mass quantity (kg) |
| $n$ | Molar quantity (kmol) |
| $c_n$ | Correlation constants (-) |
| $h$ | Specific enthalpy (kJ/kg) |
| $\Delta H_c$ | Enthalpy of combustion (kJ) |
| $X_b$ | Burned mass fraction (-) |
| $P$ | Pressure (kPa) |
| $V$ | Volume ($m^3$) |
| $V_c$ | Clearance volume ($m^3$) |
| $Q$ | Heat energy (kJ) |
| $W$ | Indicated work (kJ) |
| $U_p$ | Mean piston speed (m/s) |
| $k$ | Thermal conductivity (W/m-K) |
| $\gamma$ | Adiabatic index (-) |
| $\epsilon$ | Crank/rod length ratio (-) |
| $\mu$ | Dynamic viscosity (Pa-s) |
| $\rho$ | Density ($kg/m^3$) |
| θ | Engine crank angle (deg.) |
| $\eta$ | Indicated thermal efficiency (%) |

| | |
|---|---|
| A/F | Air to fuel mass ratio |
| imep | Indicated mean effective pressure |
| LHV | Lower heating value |
| EGR | Exhaust gas recycling |
| EGT | Exhaust gas temperature |
| HRR | Heat release rate |
| MFB | Mass burn fraction |
| CAD | Crank angle degree |
| HCCI | Homogeneous charge compression ignition |
| BTDC | Before top dead centre |
| ATDC | After top dead centre |